Letter

Parametrized quantum circuit for weight-adjustable quantum loop gas

Rong-Yang Sun, 1,2 Tomonori Shirakawa, 1,2 and Seiji Yunoki, 2,3,4

¹Computational Materials Science Research Team, RIKEN Center for Computational Science (R-CCS), Kobe, Hyogo 650-0047, Japan
²Quantum Computational Science Research Team, RIKEN Center for Quantum Computing (RQC), Wako, Saitama 351-0198, Japan
³Computational Quantum Matter Research Team, RIKEN Center for Emergent Matter Science (CEMS), Wako, Saitama 351-0198, Japan
⁴Computational Condensed Matter Physics Laboratory, RIKEN Cluster for Pioneering Research (CPR), Saitama 351-0198, Japan



(Received 26 October 2022; accepted 17 January 2023; published 25 January 2023)

Motivated by the recent success of realizing the topologically ordered ground state of the exactly solvable toric code model by a quantum circuit on the real quantum device [Satzinger et al., Science 374, 1237 (2021)], here we propose a parametrized quantum circuit (PQC) with the same real-device-performable optimal structure to represent quantum loop gas states with adjustably weighted loop configurations. Combining such a PQC with the variational quantum eigensolver, we obtain the accurate quantum circuit representation for the toric code model in an external magnetic field with any field strength, where the system is not exactly solvable. The topological quantum phase transition in this system is further observed in the optimized circuits by measuring the magnetization and topological entanglement entropy.

DOI: 10.1103/PhysRevB.107.L041109

Introduction. The topologically ordered state, a new category of exotic quantum states of matter, has continuously attracted research interest in recent decades [1–3]. Many novel properties that emerge from it include the degenerate ground state with long-range quantum entanglement and the anyonictype excitations, which are also deemed essential for the development of quantum computing [4,5]. However, because of the existence of the long-range quantum entanglement, it is challenging to investigate the topologically ordered state. Except for rare elaborately constructed exactly solvable models, such as Kitaev's toric code model [4] and Wen's plaquette model [6], it is difficult to verify whether a topologically ordered phase exists in a certain microscopic quantum manybody Hamiltonian and to identify its nature, a famous example being the spin-1/2 antiferromagnetic Heisenberg model on the kagome lattice [7-10].

On the other hand, rapidly developed synthetic controllable quantum platforms, both in circuit-based quantum computers [11,12] and analog quantum simulators [13–15], offer a new way to explore these long-range-entangled states. These controllable quantum systems have an intrinsic quantum entangled nature and thus are expected to be able to handle another quantum entangled system relatively easier. Recently, this expectation has been partially realized. One can use the optimal quantum resource to realize the ground state of the toric code model and accurately probe its properties [16], demonstrating a huge potential for utilizing quantum computers to study topologically ordered states.

Many algorithms have been proposed to efficiently use the quantum resource for solving a generic *nonexactly solvable* quantum many-body problem. Among them, the most promising one, which is considered to be realizable on current noisy-intermediate scale quantum (NISQ) devices [17,18], is the variational quantum eigensolver (VQE) [19–21]. The

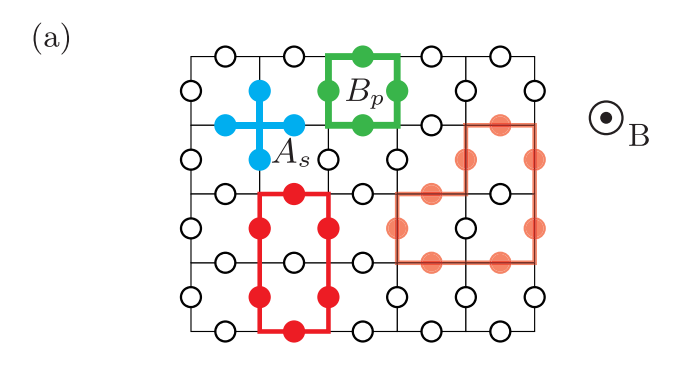
VQE adopts a parametrized quantum circuit (PQC) as the *Ansatz* state. This PQC *Ansatz* is evaluated on a quantum computer, while its parameters are optimized by a classical optimizer. Despite considerable efforts, the scalable realization of the VQE on NISQ devices is still under extensive research. This is because proper PQC *Ansätze*, which can faithfully describe the ground state of a given quantum many-body Hamiltonian and yet can be performed accurately enough on real devices, are still missing, especially when the system is close to a phase transition point (for example, see Ref. [22]).

In this Letter, we address this issue by proposing a PQC, which has adequate expressibility towards the ground state of a nonexactly solvable correlated Hamiltonian and at the same time can be faithfully evaluated on NISQ devices. We encode a quantum loop gas state with adjustably weighted loop configurations into a quantum circuit with the optimal circuit depth. The adjustable weights are controlled by circuit parameters. Using such a single PQC, we precisely reproduce the ground state with an energy accuracy better than the order of 10^{-2} for the toric code model in an external magnetic field, thus in both topologically ordered and ferromagnetically ordered phases, by VQE calculations.

Toric code model in a magnetic field. The toric code model [4] is defined by qubits located on the bond centers of a $L_x \times L_y$ square lattice with N bonds and is given by the following Hamiltonian:

$$H_{\rm TC} = -\sum_{s} A_s - \sum_{p} B_p \,, \tag{1}$$

where $A_s = \prod_{i \in s} \sigma_i^z$ and $B_p = \prod_{i \in p} \sigma_i^x$. Here, σ_i^z (σ_i^x) is the Pauli Z(X) operator of qubit i located on the ith bond center and s(p) sums over all the vertices (plaquettes) of the



(b)

$$|\Psi(\boldsymbol{\theta})\rangle = |\Psi(\boldsymbol{\theta})\rangle + |\Psi(\boldsymbol$$

FIG. 1. (a) Schematic figure of the toric code model in an external magnetic field B applied along the z direction on the 6×5 lattice under OBCs, where qubits (indicated by circles) are located on each bond of the lattice. Here, the blue cross connecting four blue circles indicates an A_s term and the green square connecting four green circles denotes a B_p term. Note that A_s terms are also present at the corners and edges of the lattice under OBCs, thus involving only two and three qubits, respectively. The loops (indicated by red) are formed by local qubit states $|1\rangle_i$, while qubits not along any loops are $|0\rangle_i$. (b) Schematic figure of the Ansatz state $|\Psi(\theta)\rangle$ generated by a parametrized loop gas circuit. In these two figures, the shade intensity of red for loops represents a weight of the corresponding loops.

underlying square lattice [see Fig. 1(a)]. The Hamiltonian in Eq. (1) is exactly solvable and its ground state is a topological quantum spin liquid characterized by a Z_2 topological order [4,23]. For the toric code model with open boundary conditions (OBCs) along the two prime directions, its unique ground state can be constructed as [16]

$$|\Psi_0\rangle = \prod_{p=1}^{N_p} \left(\frac{1}{\sqrt{2}} \mathbb{I}_p + \frac{1}{\sqrt{2}} B_p \right) |00 \cdots 0\rangle, \qquad (2)$$

where $\mathbb{I}_p = \prod_{i \in p} I_i$ is the identity operator on the *p*th plaquette $(I_i \text{ being the identity operator at qubit } i)$, N_p is the total number of the plaquettes, and $|00\cdots 0\rangle = |0\rangle_1 |0\rangle_2 \cdots |0\rangle_N$ represents a product of the local states $|0\rangle_i$ with $\sigma_i^z |0\rangle_i = |0\rangle_i$ and $\sigma_i^z |1\rangle_i = -|1\rangle_i$. Equation (2) can be interpreted as generating an equally weighted superposition of all possible basis configurations which contain only closed loops formed by local states $|1\rangle_i$, i.e., a quantum loop gas (LG).

An external magnetic field along the z direction can drive the toric code model away from the exactly solvable point and leads to a topological quantum phase transition [24,25]. The corresponding Hamiltonian [also see Fig. 1(a)] is described by

$$H_{\text{TCM}}(x) = (1 - x)H_{\text{TC}} - x \sum_{i=1}^{N} \sigma_i^z$$
. (3)

When x = 0, $H_{TCM}(x)$ returns to the toric code case, while it has the exact ground state $|00\cdots 0\rangle$ when x = 1. Extensive

quantum Mount Carlo studies have suggested that $H_{\text{TCM}}(x)$ goes through a second-order quantum phase transition at $x_c \sim 0.25$ from the toric code state to the ferromagnetically ordered state in the thermodynamic limit [25].

It is quite insightful to understand the ground state of $H_{\rm TCM}(x)$ using the LG picture and consider the magnetic field inducing tension to the loops [24]. In the presence of the magnetic field, the loop with a more extended perimeter costs more energy and its weight in the ground state should be lightened to minimize the energy, as schematically illustrated in Fig. 1(a). Therefore, an LG with adjustable weights for each loop pattern can be regarded as an appropriate description of the ground state of $H_{\rm TCM}(x)$, especially when the charge excitation is gapped out and thus closed loop configurations remain without having open strings. In the rest of this Letter, we will show how to represent this as a PQC with an optimal circuit structure.

Parametrized loop gas circuit. Before introducing the PQC for a weight-adjustable LG, we briefly recall the method to construct the ground state $|\Psi_0\rangle$ of the pure toric code model H_{TC} with an optimal quantum circuit [16,26]. The core steps to generate $|\Psi_0\rangle$ are to apply a serial of $(\mathbb{I}_p + B_p)/\sqrt{2}$ operators, which can be realized by applying a Hadamard gate H to a representative qubit associated with a plaquette and then applying CNOT gates controlled by the representative qubit to the other qubits in this plaquette. The circuit depth in this construction grows linearly with L_y , meeting the lower bound of the information spread in the quantum circuit to construct a globally entangled quantum state [27]. Furthermore, the circuit constructed by this method has been realized on the current NISQ devices with high accuracy [16].

Applying a Hadamard gate to $|0\rangle_i$ is nothing but creating the equally weighted superposition between $|0\rangle_i$ (i.e., vacuum) and $|1\rangle_i$ (a precursor of the loop). In order to construct an LG with differently weighted loop patterns, we need to create an imbalanced superposition between $|0\rangle_i$ and $|1\rangle_i$, which is rather straightforward once we notice the relation

$$H|0\rangle_i = R_y(\pi/2)|0\rangle_i,\tag{4}$$

where

$$R_{y}(\theta) = \begin{pmatrix} \cos\frac{\theta}{2} & -\sin\frac{\theta}{2} \\ \sin\frac{\theta}{2} & \cos\frac{\theta}{2} \end{pmatrix}$$
 (5)

is the rotation-y gate. When θ deviates from $\pi/2$, an imbalanced superposition, $\cos(\theta/2)|0\rangle_i + \sin(\theta/2)|1\rangle_i$, can be realized. Therefore, a PQC, with N_p parameters varying in the range $[0,2\pi)$ to represent a weight-adjustable LG state, can be constructed simply by replacing the Hadamard gates with the rotation-y gates in the construction of $|\Psi_0\rangle$ described above. Furthermore, it is straightforward to show that this PQC realizes the variational state

$$|\Psi(\boldsymbol{\theta})\rangle = \prod_{p=1}^{N_p} [\cos(\theta_p/2)\mathbb{I} + \sin(\theta_p/2)B_p] |00\cdots0\rangle, \quad (6)$$

which is restored to $|\Psi_0\rangle$ when $\theta = \{\theta_p\}_{p=1}^{N_p}$ with $\theta_p = \pi/2$. For a schematic example of $|\Psi(\theta)\rangle$, see Fig. 1(b). We call it the parametrized loop gas circuit (PLGC) since it represents a LG state with parametrizable weighted loop patterns.

Although the PLGC cannot cover all the LG with nonuniformly weighted loop patterns, we will demonstrate below that it can accurately represent the ground state of $H_{\text{TCM}}(x)$ with any magnetic field strength.

We should also note here that the performability of the PLGC on real devices has already been examined in Ref. [16] since applying a rotation-y gate has the same duration and error rate as applying a Hadamard gate on Google's sycamore quantum processor [11,28]. Furthermore, the PLGC has a solid potential to be performed on other quantum platforms where the error-correction surface codes have been realized [29–31].

VQE calculations for $H_{TCM}(x)$ using *PLGC*. To further verify that this NISQ-device-realizable PLGC can fully characterize the ground state of $H_{TCM}(x)$, we perform numerical simulations of the VQE calculations for this Hamiltonian with $x \in [0, 1]$ using the PLGC on different clusters up to N = 24, i.e., $L_x \times L_y = 4 \times 4$ with $N_p = 9$, under OBCs. These numerical simulations are based on the state vector quantum circuit simulator provided by *Oiskit* [32]. For each x with a given system size, the initial parameters θ_0 in the PLGC are assigned randomly and these parameters are updated by a simultaneous perturbation stochastic approximation (SPSA) [33] classical optimizer to minimize the expectation value of the energy. Here, the SPSA optimizer is employed simply because fewer circuit evaluations are required and thus it is suitable for real quantum device experiments. However, other gradient-based optimizers are also examined and obtain consistent results. The same procedure with a different set of random initial parameters is repeated 10 times to check that the results converge to the same state $|\Psi(\theta_{\rm opt})\rangle$ with the optimized parameter $\theta_{\rm opt}$. The physical quantities are evaluated using the optimized state $|\Psi(\theta_{\rm opt})\rangle$. For comparison, we also perform the numerically exact diagonalization (ED) calculations for the same system using the *QuSpin* library [34].

First, we find in Fig. 2 that the VQE energy E_0 is in excellent agreement with the exact energy $E_{\rm ED}$ obtained by the ED method for all magnetic field strengths on all different clusters studied. Confirming that the difference of the ground-state energy per qubit is always smaller than 10^{-2} (see the inset of Fig. 2, where the extrapolated values to $N \to \infty$ are also indicated), we conclude that the ground state of this nonexactly solvable quantum many-body system can be achieved by the VQE calculations with the PLGC *Ansatz*, which thus provides a notable improvement as compared with the recent results using the Hamiltonian variational *Ansatz* [22].

Moreover, in order to check whether the PLGC can characterize the topological quantum phase transition induced by the external magnetic field in $H_{\rm TCM}(x)$, we evaluate the expectation value of the magnetization, i.e.,

$$\langle m_z \rangle = \frac{1}{N} \sum_{i=1}^{N} \langle \sigma_i^z \rangle,$$
 (7)

where $\langle \cdots \rangle$ indicates the expectation value over the optimized PLGC state $|\Psi(\theta_{\rm opt})\rangle$ and also the topological entanglement entropy (TEE) [35,36], which identifies the existence and the nature of the topological order in $|\Psi(\theta_{\rm opt})\rangle$. Here, the TEE $S_{\rm topo}$ is defined by the residual quantum mutual information in

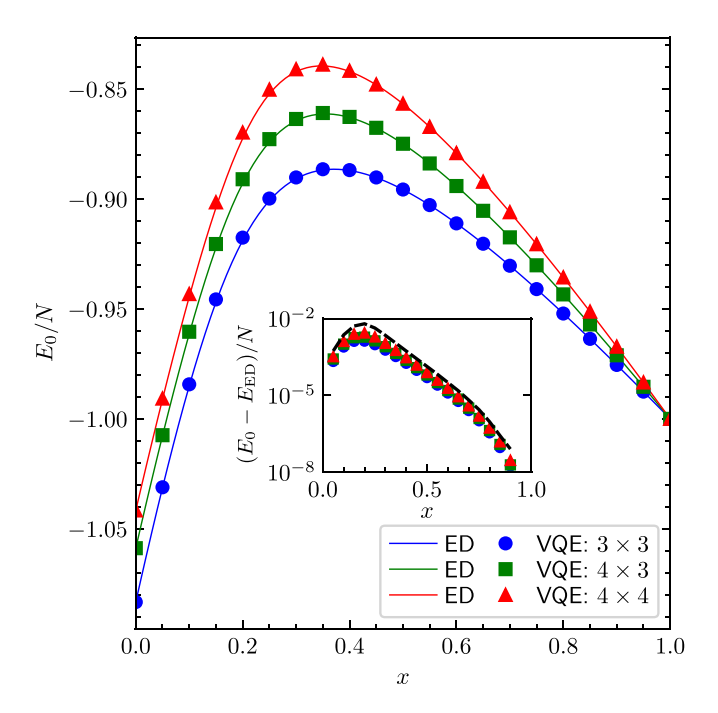


FIG. 2. Ground state energy E_0 obtained by the VQE calculations as a function of x for $H_{\text{TCM}}(x)$ on different clusters, $L_x \times L_y = 3 \times 3$, 4×3 , and 4×4 (indicated by blue circles, green squares, and red triangles, respectively), which correspond to N (N_p) = 12 (4), 17 (6), and 24 (9), respectively (also see the insets of Fig. 4). For comparison, the ground-state energy E_{ED} obtained by the ED method are also plotted by solid lines with the same colors. The inset shows the corresponding energy difference per qubit, $\Delta e_0 \equiv (E_0 - E_{\text{ED}})/N$, indicated by the same symbols. The dashed line displays the extrapolated values of Δe_0 to $N \to \infty$ estimated by fitting Δe_0 for the three different clusters with a second-order polynomial of 1/N.

a tripartite subsystem,

$$S_{\text{topo}} = S_{\text{A}} + S_{\text{B}} + S_{\text{C}} - S_{\text{AB}} - S_{\text{BC}} - S_{\text{AC}} + S_{\text{ABC}},$$
 (8)

where S_X is the entanglement entropy between subsystem X and the rest of the system, and A, B, and C are the three subregions in the tripartite subsystem (see the inset of Fig. 4). S_{topo} is equal to $-\ln 2$ in the toric code state, revealing its Z_2 topologically ordered nature [23]. For the numerical simulations, the TEE is easily extracted from the reduced density matrix. For the real device experiments, it can also be detected efficiently by recently introduced random measurement methods [37–39].

Figures 3 and 4 show the results of $\langle m_z \rangle$ and S_{topo} , respectively, which are also in good accordance with the ED results. With increasing the system size, these quantities exhibit sharper changes near the transition point expected around x=0.25, implying a phase transition in the thermodynamic limit. On the other hand, we observe that deviations of the VQE results from the ED values are most distinguishable near the transition region (also see the inset of Fig. 2 for the ground-state energy). However, this does not necessarily imply that the PLGC loses its expressibility for the phase transition in larger systems since these small clusters considered here have relatively strong finite-size effects and thus it is not

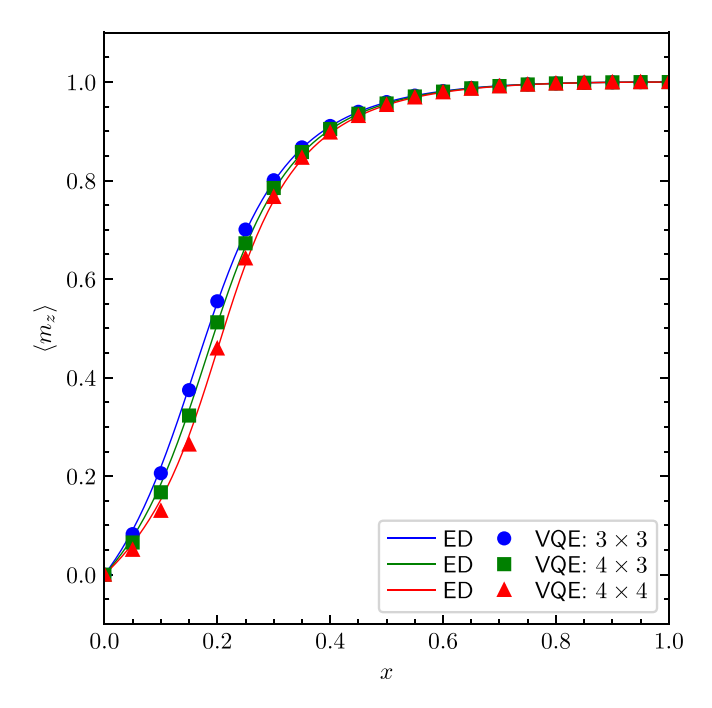


FIG. 3. Same as Fig. 2 but for the ground-state magnetization $\langle m_z \rangle$.

conclusive how these results converge in the thermodynamics limit, which is left for future study.

Conclusion and discussion. In summary, we have proposed a parametrized quantum circuit, PLGC, which can represent a class of quantum loop gas states with adjustable weights and maintain the same optimal circuit structure as that for constructing the ground state of the toric code model. Therefore, the PLGC can be performed on the current NISQ devices with high accuracy. Furthermore, using the PLGC, we have performed the VQE calculations of the toric code model in the presence of the external magnetic field and demonstrated that a very accurate ground state can be obtained for any field strength. Moreover, the topological quantum phase transition between the Z_2 topologically ordered state and the ferromagnetically ordered state is displayed by evaluating the magnetization and the topological entanglement entropy of the optimized PLGC, which are also highly compatible with the numerically exact results.

The dramatic performance improvement of the VQE calculations provided by the use of the PLGC, as compared with the VQE calculations using Hamiltonian-variational-type *Ansätze* [40], which also includes the quantum alternating operator

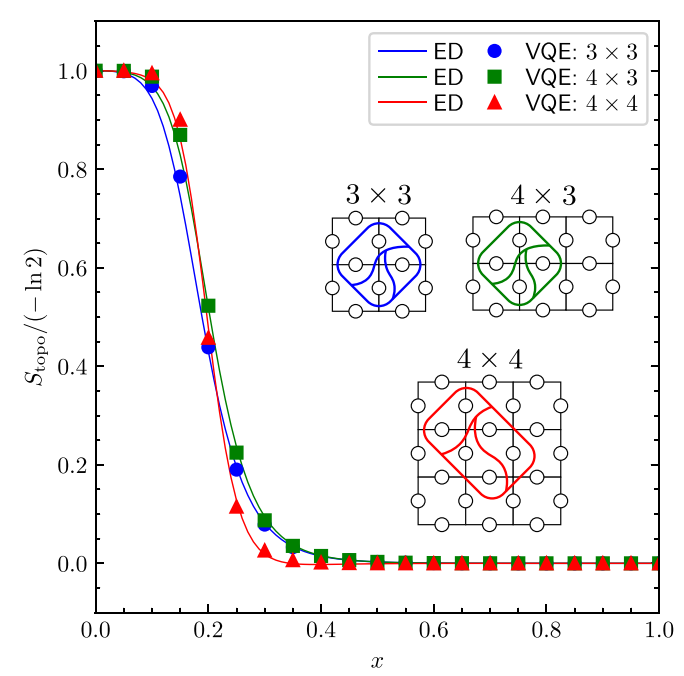


FIG. 4. Same as Fig. 2 but for the ground-state TEE S_{topo} . The insets show the subsystems with the tripartition to extract S_{topo} for the corresponding systems.

Ansatz [41], is owing to its more precise description of the low-lying physical Hilbert space. For instance, the imaginary part of an Ansatz state, which is unnecessary to describe the ground state of $H_{\rm TCM}(x)$ but is inevitably introduced by time evolution operations in Hamiltonian-variational-type Ansätze, can be perfectly avoided in the PLGC. This insight sheds light on how to maximally utilize current NISQ devices for solving quantum many-body problems.

Acknowledgments. We are grateful to K. Nagao for helpful discussions. Parts of numerical simulations have been done on the HOKUSAI supercomputer at RIKEN (Project ID No. Q22577) and the supercomputer Fugaku installed in RIKEN R-CCS (Project ID No. hp220217). This work is supported by Grant-in-Aid for Scientific Research (A) (No. JP21H04446) and Grant-in-Aid for Scientific Research (C) (No. JP22K03479) from MEXT, Japan, and also by JST COI-NEXT (Grant No. JPMJPF2221). This work is also supported in part by the COE research grant in computational science from Hyogo Prefecture and Kobe City through the Foundation for Computational Science.

^[1] D. C. Tsui, H. L. Stormer, and A. C. Gossard, Phys. Rev. Lett. 48, 1559 (1982).

^[2] X.-G. Wen, Int. J. Mod. Phys. B 04, 239 (1990).

^[3] X.-G. Wen, Rev. Mod. Phys. 89, 041004 (2017).

^[4] A. Kitaev, Ann. Phys. (NY) 303, 2 (2003).

^[5] C. Nayak, S. H. Simon, A. Stern, M. Freedman, and S. Das Sarma, Rev. Mod. Phys. 80, 1083 (2008).

^[6] X.-G. Wen, Phys. Rev. Lett. 90, 016803 (2003).

^[7] G. Evenbly and G. Vidal, Phys. Rev. Lett. 104, 187203 (2010).

^[8] S. Yan, D. A. Huse, and S. R. White, Science 332, 1173 (2011).

^[9] Y.-C. He, M. P. Zaletel, M. Oshikawa, and F. Pollmann, Phys. Rev. X 7, 031020 (2017).

^[10] R.-Y. Sun, H.-K. Jin, H.-H. Tu, and Y. Zhou, arXiv:2203.07321.

^[11] F. Arute, K. Arya, R. Babbush, D. Bacon, J. C. Bardin, R. Barends, R. Biswas, S. Boixo, F. G. Brandao, D. A. Buell *et al.*, Nature (London) **574**, 505 (2019).

- [12] I. Pogorelov, T. Feldker, C. D. Marciniak, L. Postler, G. Jacob, O. Krieglsteiner, V. Podlesnic, M. Meth, V. Negnevitsky, M. Stadler, B. Höfer, C. Wächter, K. Lakhmanskiy, R. Blatt, P. Schindler, and T. Monz, PRX Quantum 2, 020343 (2021).
- [13] C. Gross and I. Bloch, Science 357, 995 (2017).
- [14] F. Schäfer, T. Fukuhara, S. Sugawa, Y. Takasu, and Y. Takahashi, Nat. Rev. Phys. 2, 411 (2020).
- [15] Y. Takahashi, Proc. Jpn. Acad., Ser. B 98, 141 (2022).
- [16] K. J. Satzinger, Y.-J. Liu, A. Smith, C. Knapp, M. Newman, C. Jones, Z. Chen, C. Quintana, X. Mi, A. Dunsworth, C. Gidney, I. Aleiner, F. Arute, K. Arya, J. Atalaya, R. Babbush, J. C. Bardin, R. Barends, J. Basso, A. Bengtsson *et al.*, Science 374, 1237 (2021).
- [17] J. Preskill, Quantum 2, 79 (2018).
- [18] K. Bharti, A. Cervera-Lierta, T. H. Kyaw, T. Haug, S. Alperin-Lea, A. Anand, M. Degroote, H. Heimonen, J. S. Kottmann, T. Menke, W.-K. Mok, S. Sim, L.-C. Kwek, and A. Aspuru-Guzik, Rev. Mod. Phys. 94, 015004 (2022).
- [19] A. Peruzzo, J. McClean, P. Shadbolt, M.-H. Yung, X.-Q. Zhou, P. J. Love, A. Aspuru-Guzik, and J. L. O'brien, Nat. Commun. 5, 4213 (2014).
- [20] M.-H. Yung, J. Casanova, A. Mezzacapo, J. Mcclean, L. Lamata, A. Aspuru-Guzik, and E. Solano, Sci. Rep. 4, 3589 (2014).
- [21] M. Cerezo, A. Arrasmith, R. Babbush, S. C. Benjamin, S. Endo, K. Fujii, J. R. McClean, K. Mitarai, X. Yuan, L. Cincio, and P. J.Coles, Nat. Rev. Phys. 3, 625 (2021).
- [22] K. N. Okada, K. Osaki, K. Mitarai, and K. Fujii, arXiv:2202.02909.
- [23] A. Kitaev, Ann. Phys. (NY) 321, 2 (2006).
- [24] S. Trebst, P. Werner, M. Troyer, K. Shtengel, and C. Nayak, Phys. Rev. Lett. 98, 070602 (2007).
- [25] F. Wu, Y. Deng, and N. Prokof'ev, Phys. Rev. B **85**, 195104 (2012).

- [26] Y.-J. Liu, K. Shtengel, A. Smith, and F. Pollmann, PRX Quantum 3, 040315 (2022).
- [27] S. Bravyi, M. B. Hastings, and F. Verstraete, Phys. Rev. Lett. 97, 050401 (2006).
- [28] T. I. Andersen, Y. D. Lensky, K. Kechedzhi, I. Drozdov, A. Bengtsson, S. Hong, A. Morvan, X. Mi, A. Opremcak, R. Acharya et al., arXiv:2210.10255.
- [29] S. Krinner, N. Lacroix, A. Remm, A. Di Paolo, E. Genois, C. Leroux, C. Hellings, S. Lazar, F. Swiadek, J. Herrmann *et al.*, Nature (London) 605, 669 (2022).
- [30] Y. Zhao, Y. Ye, H.-L. Huang, Y. Zhang, D. Wu, H. Guan, Q. Zhu, Z. Wei, T. He, S. Cao, F. Chen, T.-H. Chung, H. Deng, D. Fan, M. Gong, C. Guo, S. Guo, L. Han, N. Li, S. Li *et al.*, Phys. Rev. Lett. **129**, 030501 (2022).
- [31] N. Sundaresan, T. J. Yoder, Y. Kim, M. Li, E. H. Chen, G. Harper, T. Thorbeck, A. W. Cross, A. D. Córcoles, and M. Takita, arXiv:2203.07205.
- [32] Qiskit, https://www.qiskit.org/
- [33] J. Spall, IEEE Trans. Autom. Control 37, 332 (1992).
- [34] P. Weinberg and M. Bukov, SciPost Phys. 2, 003 (2017).
- [35] A. Kitaev and J. Preskill, Phys. Rev. Lett. 96, 110404 (2006).
- [36] M. Levin and X.-G. Wen, Phys. Rev. Lett. 96, 110405 (2006).
- [37] S. J. van Enk and C. W. J. Beenakker, Phys. Rev. Lett. 108, 110503 (2012).
- [38] A. Elben, B. Vermersch, M. Dalmonte, J. I. Cirac, and P. Zoller, Phys. Rev. Lett. 120, 050406 (2018).
- [39] T. Brydges, A. Elben, P. Jurcevic, B. Vermersch, C. Maier, B. P. Lanyon, P. Zoller, R. Blatt, and C. F. Roos, Science 364, 260 (2019).
- [40] D. Wecker, M. B. Hastings, and M. Troyer, Phys. Rev. A 92, 042303 (2015).
- [41] S. Hadfield, Z. Wang, B. O'Gorman, E. G. Rieffel, D. Venturelli, and R. Biswas, Algorithms 12, 34 (2019).